

Coherent dynamics of a photon-dressed qubit

C.-H. Chien,^{1,*} M. P. Liul,^{2,†} C.-Y. Chen,¹ P. Y. Wen,³ J. C. Chen,^{1,4}
Y.-H. Lin,^{1,4} S. N. Shevchenko,^{2,5} Franco Nori,^{6,7,8} and I.-C. Hoi^{9,1,‡}

¹*Department of Physics, National Tsing Hua University, Hsinchu 30013, Taiwan*

²*B. Verkin Institute for Low Temperature Physics and Engineering, Kharkov 61103, Ukraine*

³*Department of Physics, National Chung Cheng University, Chiayi 621301, Taiwan*

⁴*Center for Quantum Technology, National Tsing Hua University, Hsinchu 30013, Taiwan*

⁵*V. N. Karazin Kharkiv National University, Kharkov 61022, Ukraine*

⁶*Theoretical Quantum Physics Laboratory, Cluster for Pioneering Research, RIKEN, Wakoshi, Saitama 351-0198*

⁷*Quantum Computing Center, RIKEN, Wakoshi, Saitama 351-0198, Japan*

⁸*Department of Physics, The University of Michigan, Ann Arbor, MI 48109-1040, USA*

⁹*Department of Physics, City University of Hong Kong,
Tat Chee Avenue, Kowloon, Hong Kong SAR, China*

(Dated: March 28, 2025)

We consider the dynamics and stationary regime of a capacitively-shunted transmon-type qubit in front of a mirror, affected by two signals: probe and dressing signals. By varying the parameters of these signals and then analyzing the probe signal (reflected by the atom-mirror system), it is possible to explore the system dynamics, which can be described by the Bloch equation. The obtained time-dependent occupation probabilities are related to the experimentally measured reflection coefficient. The study of this type of dynamics opens up new horizons for better understanding of the system properties and underlying physical processes, such as Landau-Zener-Stückelberg-Majorana transitions.

I. INTRODUCTION

Topics related to quantum computing are attracting considerable attention [1–5]. One of the most promising building blocks of such devices are superconducting qubits (see, e.g., [6–8]). These can be operated at nanosecond scales with sub-milli-second coherence times [9], are controlled by microwaves and have lithographic scalability [10]. Therefore, investigations of superconducting qubits could help the development of quantum computers. For instance, for the improved implementation of various logic gate operations [11] and quantum algorithms [12].

A superconducting qubit in a semi-infinite transmission line [13] is important for quantum electrodynamics, especially waveguide quantum electrodynamics (WQED) [14, 15]. For example, in Ref. [16] it was found that a transmon qubit embedded at the end of a transmission line can amplify a probe signal with an amplitude gain of up to 7%; while a single quantum dot [17] and natural atoms [18] show the signal amplifications at much lower levels: 0.005% and 0.4%, respectively. The investigation of our system could also address some of the existing problems in WQED, including: dynamics in atom-like mirrors [19], collective Lamb shift [20], generation of non-classical microwaves [21], dynamical Casimir effect [22], cross-Kerr effect [23], photon routing [24], probabilistic motional averaging [25], etc.

Another exciting area of research involves the study of Landau-Zener-Stückelberg-Majorana (LZSM) interferometry [26–29]. LZSM transitions are observed if a two-level system is driven back and forth by a periodic signal with a frequency close to the system resonant frequency. The importance of LZSM interferometry for controlling

quantum dynamics was studied in Refs. [29–35].

Reference [36] explored LZSM interferometry in an atom-mirror system, but only in the stationary regime. Therefore, those results were in the frequency domain. The temporal dynamics of LZSM interferometry has been unexplored. Here, in this work, we study the dynamics of an atom-mirror system, which provides insight on the dynamics of LZSM interferometry.

The rest of the paper is organized as follows. Sec. II is devoted to the description of the experiment. In Sec. III the theoretical aspects of the problem are described; we introduce the Hamiltonian of the system and the equation of motion which was solved to obtain all considered dependencies. Sec. IV presents our results: the comparison of the theory and the experiment is given; the general patterns of the system are described and explained. In Sec. V we present our conclusions.

II. EXPERIMENT

Our device consists of a transmon qubit, embedded at a distance ($L \simeq 33$ mm, where the resonant frequency corresponds to 1.84λ) of a semi-one-dimensional transmission line with characteristic impedance $Z_0 \simeq 50 \Omega$, as shown in Fig. 1 (a,b). Figure 1 (c) presents the SQUID loop of the qubit from which it can be deduced that this qubit is flux tunable. We only consider the lowest two energy levels of the transmon, and neglect all the higher levels. The energy splitting of the two-level atom is $\hbar\omega_{10}(\Phi) \approx \sqrt{8E_J(\Phi)E_C} - E_C$, with charging energy E_C (which is approximately equal to the anharmonicity), $E_C = e^2/2C_\Sigma$, where e is the elementary charge and C_Σ is the total capacitance of the transmon, and

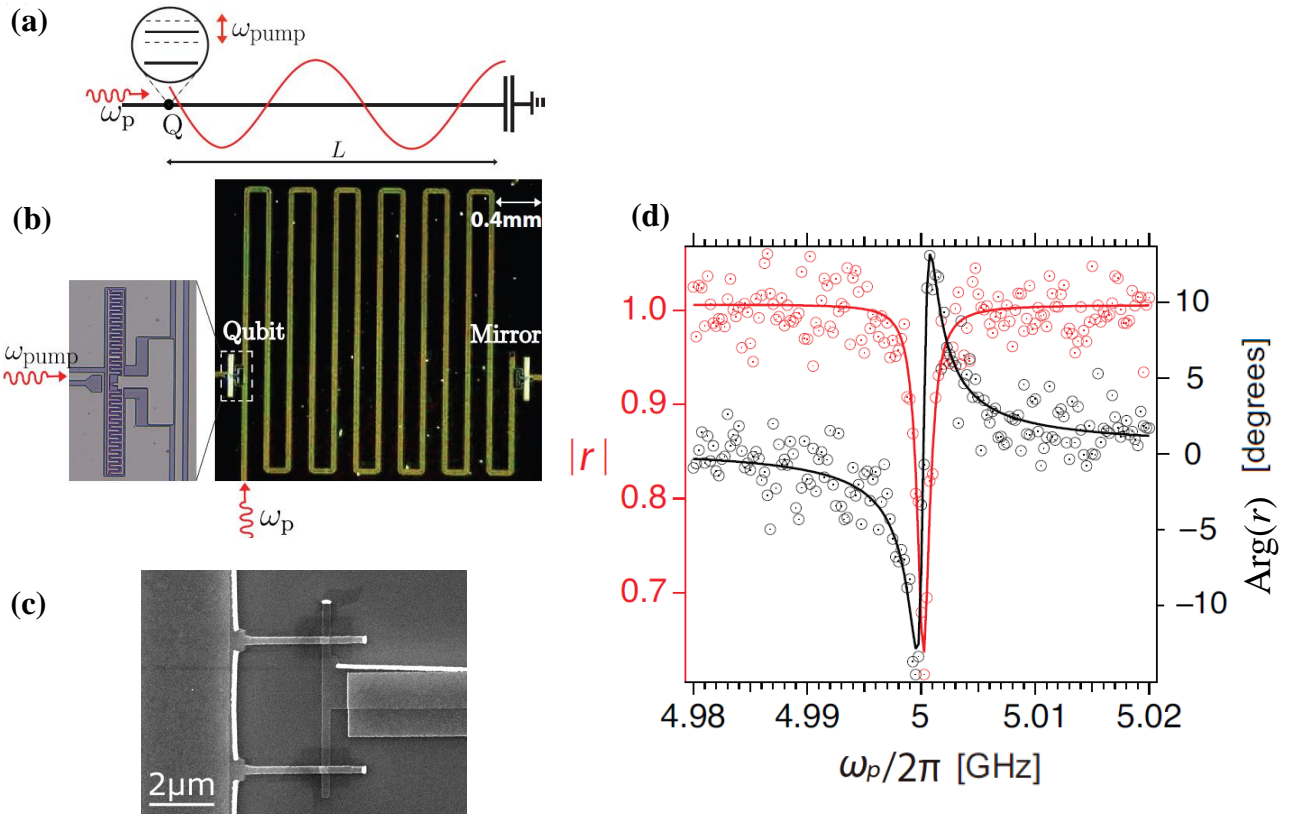


Figure 1: Device and its characterization. (a) Conceptual sketch of the device: a two-level atom, point-like object (denoted by Q), is coupled to a semi-infinite transmission line waveguide. The atom is located at a distance $L \simeq 33$ mm (1.84λ) away from the mirror (capacitance). A pump tone with frequency ω_{pump} is applied to modulate the transition frequency of the two-level atom. A weak probe tone with frequency ω_p is applied to the atom-mirror system to measure the reflection coefficient. (b) Micrographs of the device. The magnification of the distant qubit is shown to the left, where the superconducting qubit is intentionally designed to be weakly coupled to the transmission line. The weak coupling enables us to measure the temporal dynamics with a nano-second digitizer. This is the main difference between this work and a previous one [36] which focused on the stationary regime. (c) The SQUID loop of the qubit which shows that the qubit is flux tunable. (d) Reflection coefficient (magnitude response in red and phase response in black) as a function of probe frequency for a weak probe (-166 dBm). Data is shown by circles and the solid curves are the fit, using a similar fitting method as in Ref. [37].

the Josephson energy E_J , which can be tuned by the external magnetic flux Φ of a magnetic coil. The detailed measurement setup is the same as in Ref. [36].

A. Characterizing the qubit by single-tone scattering with a weak probe

First, we characterize our qubit by single-tone scattering with a weak probe, see Fig. 1(d). Fitting the magnitude and phase response of the reflection coefficient r by using the circle fit equation Eq. (1) [38] one could extract the resonant frequency ω_{10} , the relaxation rate Γ_1 and decoherence rate Γ_2 :

$$r = 1 - \frac{\Gamma_1}{\Gamma_2 + i(\omega_p - \omega_{10})}, \quad (1)$$

here r is defined as the reflected field amplitude divided by the incoming field amplitude. The extracted values

are the following: $\omega_{10} = 2\pi \times 5$ GHz, $\Gamma_1 = 2\pi \times 0.28$ MHz, and $\Gamma_2 = 2\pi \times 0.75$ MHz. These parameters will be used in the theory later. Note that we assume the incoming amplitude to be the same as the reflected amplitude when the qubit is detuned. By using two-tone spectroscopy, we know the E_C/h (anharmonicity) = 220 MHz (data not shown), which is much larger than any Rabi frequency in this work, and our two-level atom assumption is valid. From ω_{10} and E_C , we know $E_J/h = 15.5$ GHz.

B. Reflection coefficient versus pump power and probe frequency

Second, we apply both probe and dressing (pump) signals to the transmission line and the on-chip flux line (which modulates the transition frequency of the qubit), respectively. We then measure the reflection coefficient r in the (steady state) frequency domain. Both frequency

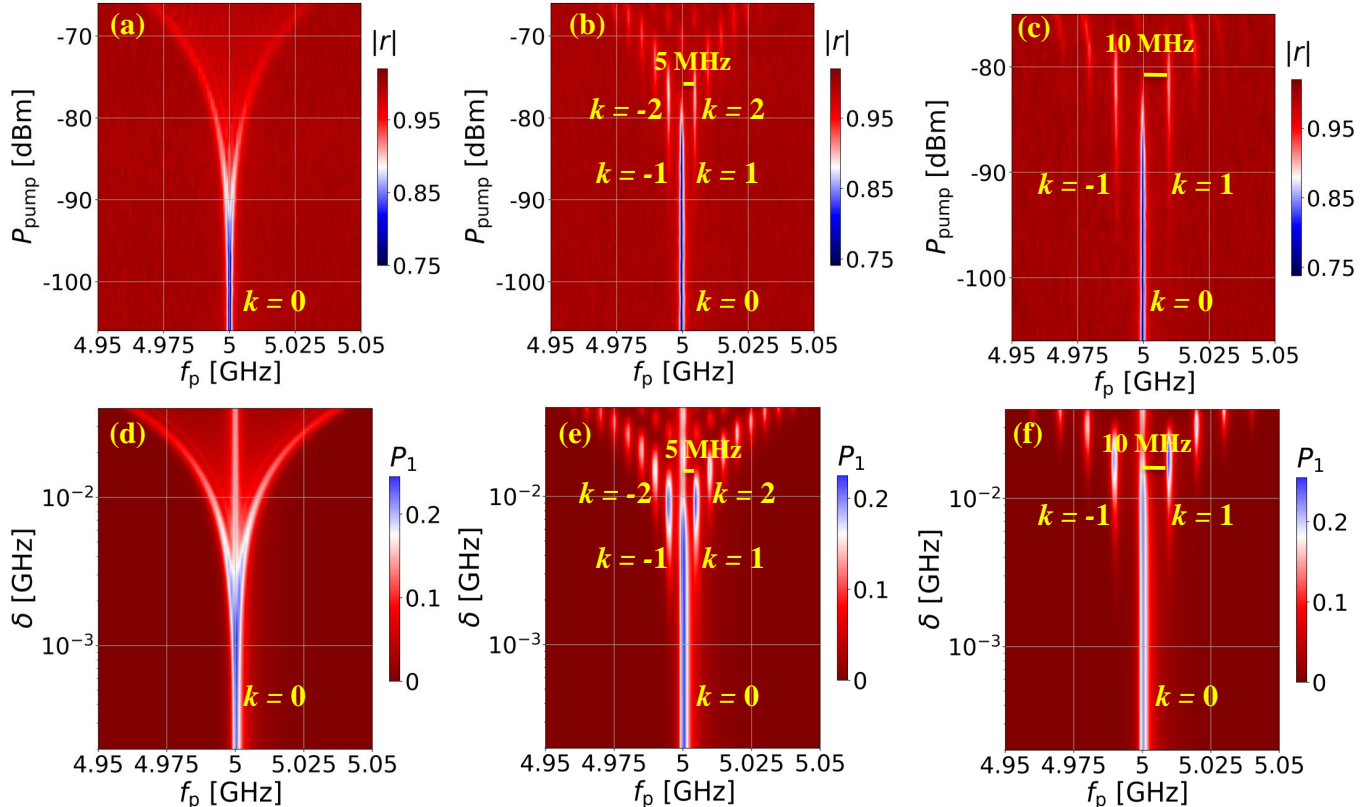


Figure 2: LZSM interferograms. These are shown via the dependence of the reflection coefficient $|r|$ on the pump power P_{pump} and probe frequency f_p at fixed pump frequency f_{pump} for a weak probe $P_p = -152$ dBm in the top panels (a,b,c) for the experimental measurements. While the bottom panels (d,e,f) show the theoretically calculated upper-level occupation probability P_1 as a function of the probe frequency f_p and the pump amplitude δ for $G(f_p = 5 \text{ GHz}) = 2\pi \times 0.7 \text{ MHz}$. The qubit is irradiated by a pump with frequency (a) $f_{\text{pump}} = 1 \text{ MHz}$, (b) $f_{\text{pump}} = 5 \text{ MHz}$, (c) $f_{\text{pump}} = 10 \text{ MHz}$. In (c), the drift on multi-photon resonance at high power is due to flux drift.

and power for the pump tone and probe tone are all tunable. Here, we scan the frequency of probe f_p , frequency of pump f_{pump} , power of pump P_{pump} , and measure the reflection coefficient $|r|$ with a fixed power of the weak probe tone. The results are shown in Fig. 2. In each subplot of Fig. 2, we fix the pump frequency, vary the pump power (y -axis) and probe frequency (x -axis). We see a LZSM interferometry pattern, where we clearly observe multi-photon resonances, which occur at $\omega_p - \omega_{10} \equiv \Delta\omega = k\omega_{\text{pump}}$.

As shown in Fig. 2(b), the higher pump power is the more resolved sidebands are visible up to $k = \pm 5$. The experimental LZSM interferometry pattern shown in Fig. 2(a,b,c) matches very well with the theory in Fig. 2(d,e,f). Detailed calculations are shown in Sec. III. Since we are using a weak probe, the upper-level occupa-

tion probability P_1 is low.

C. Temporal dynamics of the atom-mirror under both pump and probe signals

Next, we study the time dynamics of the atom-mirror system under both probe and dressing (pump) signals. In particular, we send a probe square pulse (Gaussian rise ~ 10 ns) to the transmission line and continuous sinusoidal wave pump to the on-chip flux line. We measure the reflection coefficient as a function of time and probe the frequency for a weak probe under the influence of a fixed pump power and fixed pump frequency.

In Fig. 3, each plot is taken at a fixed pump frequency and fixed pump power. The probe pulse starts at the

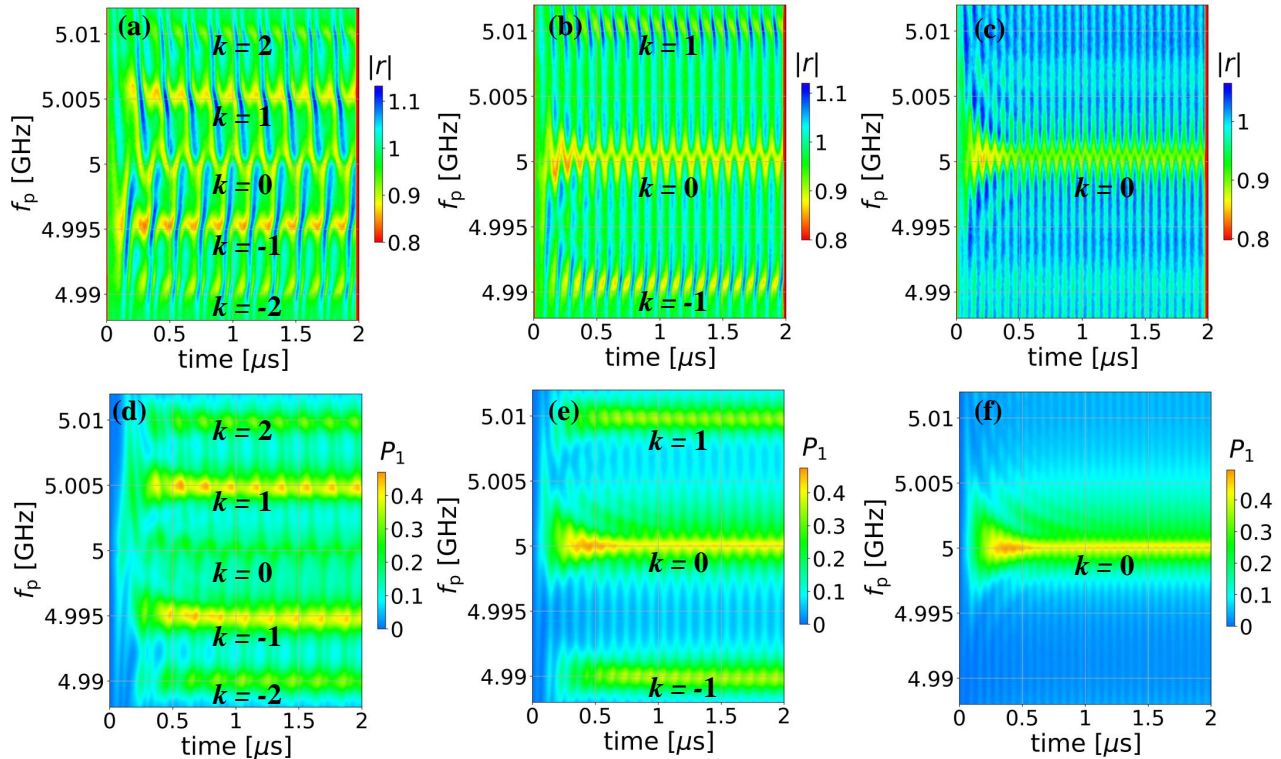


Figure 3: Coherent dynamics of the transmon qubit: dependence of the reflection coefficient $|r|$ (the upper-level occupation probability P_1) using the probe power $P_p = -146$ dBm [$G(f_p = 5 \text{ GHz}) = 2\pi \times 1.4 \text{ MHz}$] and the pump power $P_{\text{pump}} = -78.5$ dBm ($\delta = 10 \text{ MHz}$) on the probe frequency f_p and time t . Plots (a,b,c) present experimental results, (d,e,f) show plots built by data computed theoretically. The qubit is irradiated by a pump with frequency (a) $f_{\text{pump}} = 5 \text{ MHz}$, (b) $f_{\text{pump}} = 10 \text{ MHz}$, (c) $f_{\text{pump}} = 15 \text{ MHz}$. Panels (d-f) show the corresponding data computed theoretically for the qubit upper-level occupation probabilities P_1 .

beginning of the plot at $t = 0$. In Fig. 3 (a,b,c) the reflection coefficient reveal a transient dynamics starting at $t = 0$. In addition, we see the time dynamics of the multi-photon resonances, which occur at $\Delta\omega = k\omega_{\text{pump}}$, labelled by $k = -2, -1, 0, +1, +2$. And the multi-photon resonances are slightly asymmetric around $k = 0$. All of these features are consistent with the theory described in Sec. III. In Fig. 4, by taking line cuts of Fig. 3, we show detailed features of the transient at various fixed pump frequencies f_{pump} . Moreover, in Fig. 5, we also fix the pump frequency to 10 MHz and vary the pump power in (a,b,c). We see the multi-photon resonances, occurred at $k = -1, +1$, becoming weaker and weaker from (a) to (c), as the pump power decreases.

In Fig. 4, we can see the line cut along Fig. 3 at $f_p = 5 \text{ GHz}$. For a clearer comparison between theory and experiment, the y -axis for the theoretical plots was cropped and inverted. We see the transient dynamics

(around $T_2 = 1/\Gamma_2 \sim 212 \text{ ns}$) for $f_{\text{pump}} = 15 \text{ MHz}$, where $T_2 > 1/f_{\text{pump}}$ in Fig. 4(c). When $T_2 \sim 1/f_{\text{pump}}$, the transient dynamics is not clear, as shown in Fig. 4(a). In the steady state, the period of oscillations is the inverse of the pump frequency, as expected. The theory plots show the upper-level occupation probability P_1 , where the transient dynamics is around $T_1 = 1/\Gamma_1 \sim 568 \text{ ns}$. Also, for better understanding of the pump signal influence on the system dynamics, we measure the dependence of the reflection coefficient $|r|$ for no flux pump. The corresponding plots are presented in Fig. 6 in the Appendix.

III. THEORETICAL DESCRIPTION

In Ref. [36], the experimentally measured reflection coefficient $|r|$ is associated with the theoretically calculated probability of an upper level occupation P_1 (increase of

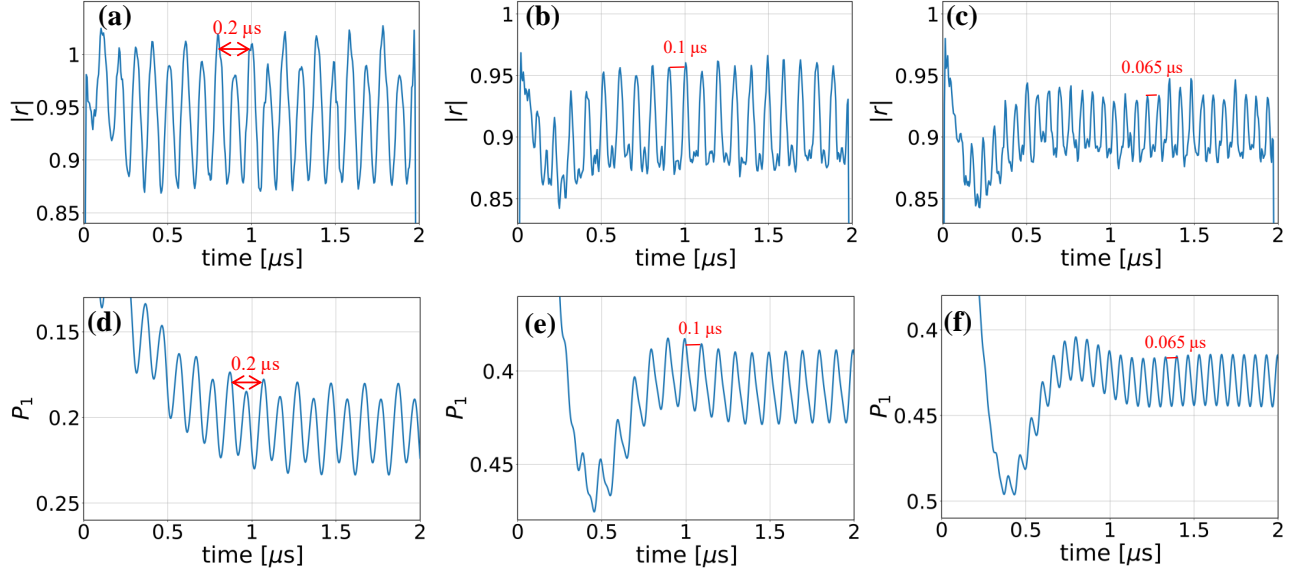


Figure 4: [Line cut of Fig. 3 along $f_p = 5$ GHz] Coherent dynamics of the transmon qubit: dependence of the reflection coefficient $|r|$ (the upper-level occupation probability P_1) on the time t at fixed pump frequency f_{pump} with $f_p = 5$ GHz, $P_p = -146$ dBm ($G(f_p = 5 \text{ GHz}) = 2\pi \times 1.4 \text{ MHz}$), $P_{\text{pump}} = -78.5$ dBm ($\delta = 10$ MHz). Plots (a,b,c) present experimental results, while panels (d,e,f) show plots computed theoretically. The qubit is irradiated by a signal with frequency (a) $f_{\text{pump}} = 5$ MHz, (b) $f_{\text{pump}} = 10$ MHz, (c) $f_{\text{pump}} = 15$ MHz. Panels (d,e,f) show the corresponding data computed theoretically for the qubit upper-level occupation probabilities P_1 . For a clearer comparison between theory and experiments, the y -axis of the theoretical plots in (d,e,f) was cropped and inverted.

P_1 corresponds to decrease of $|r|$. The computations were done in the diabatic (charge) basis. Here we use the same correspondence between theory and experiment and make our calculations in the diabatic basis. Reference. [36] showed that the system can be described by the Hamiltonian:

$$H = -\frac{B_z}{2}\sigma_z - \frac{B_x}{2}\sigma_x, \quad (2)$$

where the diagonal part corresponds to the energy-level modulation

$$B_z/\hbar = \omega_{10} + \delta \sin \omega_{\text{pump}}t, \quad (3)$$

the off-diagonal part characterizes the coupling to the probe signal

$$B_x/\hbar = G \sin \omega_p t. \quad (4)$$

To remove the fast driving from the Hamiltonian, the authors of Ref. [36] performed the unitary transformation $U = \exp(-i\omega_p \sigma_z t/2)$ and the rotating-wave approximation [39, 40] to obtain the new Hamiltonian

$$H_1 = -\frac{\hbar\widetilde{\Delta\omega}}{2}\sigma_z + \frac{\hbar G}{2}\sigma_x, \quad (5)$$

where

$$\widetilde{\Delta\omega} = \Delta\omega + f(t), \quad (6)$$

$$\Delta\omega = \omega_p - \omega_{10}, \quad (7)$$

$$f(t) = \delta \sin \omega_{\text{pump}}t. \quad (8)$$

Here δ is the amplitude of the energy-level modulation, G characterizes the coupling to the probe signal (Rabi frequency of the probe signal). According to Ref. [36]

$$G = \frac{\omega_p - \omega_{\text{node}}}{\omega_{\text{node}}} G_0, \quad (9)$$

where ω_{node} describes the qubit position in a semi-infinite transmission line, and G_0 is a value proportional to the probe signal amplitude. Such a dependence causes the asymmetry about the line $f_p = 5$ GHz in Figs. 2, 3, 5. For the current experiment $\omega_{\text{node}} = 2\pi \times 4.38$ GHz. Moreover, one can see that if $\omega_p = \omega_{\text{node}}$ the qubit is “hidden” or “decoupled” from the transmission line.

In order to describe the qubit dynamics, we use the Lindblad equation, which in the diabatic basis with the Hamiltonian (5) has a form:

$$\frac{d\rho}{dt} = -\frac{i}{\hbar} [\widehat{H}_1, \rho] + \sum_{\alpha} \check{L}_{\alpha}[\rho], \quad (10)$$

where $\rho = \begin{pmatrix} \rho_{00} & \rho_{01} \\ \rho_{01}^* & 1 - \rho_{00} \end{pmatrix}$ is the density matrix, such that $P_1 = 1 - \rho_{00}$, \check{L}_{α} is the Lindblad superoperator, which characterizes the system relaxation caused by interaction with the environment,

$$\check{L}_{\alpha}[\rho] = L_{\alpha}\rho L_{\alpha}^{\dagger} - \frac{1}{2} \{L_{\alpha}^{\dagger}L_{\alpha}, \rho\}, \quad (11)$$

where $\{a, b\} = ab + ba$ is the anticommutator. For the qubit (or generally speaking for any two-level system)

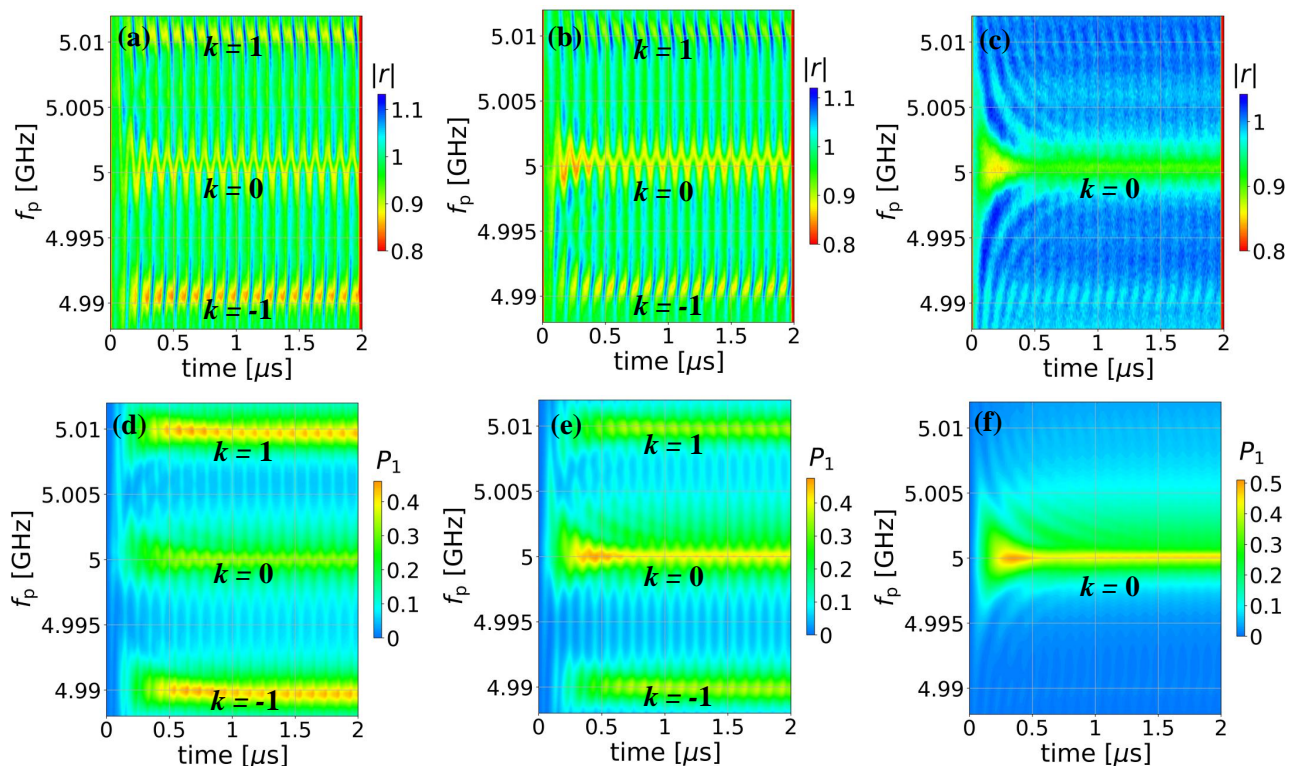


Figure 5: Coherent dynamics of the transmon qubit: dependence of the reflection coefficient $|r|$ (the upper-level occupation probability P_1) versus time t , using the probe power $P_p = -146$ dBm [$G(f_p = 5 \text{ GHz}) = 2\pi \times 1.4 \text{ MHz}$ for the theory] on the probe frequency f_p . Plots (a,b,c) present experimental results; while (d,e,f) show plots built by data computed theoretically. The qubit is irradiated by a pump signal with frequency $f_{\text{pump}} = 10 \text{ MHz}$ and power (a) $P_{\text{pump}} = -74.1 \text{ dBm}$, (b) $P_{\text{pump}} = -78.5 \text{ dBm}$, (c) $P_{\text{pump}} = -101 \text{ dBm}$. The theoretical results from the qubit upper-level occupation probability P_1 are shown for $\delta = 16.6 \text{ MHz}$ in (d), for $\delta = 10 \text{ MHz}$ in (e), and for $\delta = 0.75 \text{ MHz}$ in (f).

there are two possible relaxation channels: energy relaxation (described by L_{relax}) and dephasing (described by L_ϕ). The corresponding operators can be expressed in the following form:

$$L_{\text{relax}} = \sqrt{\Gamma_1} \sigma^+, \quad L_\phi = \sqrt{\frac{\Gamma_\phi}{2}} \sigma_z \quad (12)$$

with $\sigma^+ = \begin{pmatrix} 0 & 1 \\ 0 & 0 \end{pmatrix}$, $\sigma_z = \begin{pmatrix} 1 & 0 \\ 0 & -1 \end{pmatrix}$, Γ_1 being the qubit relaxation, $\Gamma_2 = \Gamma_1/2 + \Gamma_\phi$ is the decoherence rate, Γ_ϕ is the pure dephasing rate.

IV. INTERFEROMETRY AND DYNAMICS

By solving Eq. (10) we obtain P_1 as a function of time t , pump frequency $f_{\text{pump}} = \omega_{\text{pump}}/2\pi$, pump power P_{pump} (corresponds to δ in theory), probe frequency $f_p = \omega_p/2\pi$, probe power P_p (corresponds to G in theory). The occupation probability is the function of all these parameters, $P_1 = P_1(t, f_{\text{pump}}, f_p, \delta, G)$. The dependence obtained allows us to build, for instance, $P_1 = P_1(f_p, t)$. Also we can compute the dependencies

for P_1 in a stationary regime by making the time averaging of the results.

Figure 2 shows a time-averaged interferogram, where P_1 is a function of P_{pump} and f_p . We use the extracted parameters in Fig. 1(d), and select $G(f_p = 5 \text{ GHz}) = 2\pi \times 0.7 \text{ MHz}$ in Fig. 2; $G(f_p = 5 \text{ GHz}) = 2\pi \times 1.4 \text{ MHz}$ in Figs. 3, 4, 5, 6 (calibration between Rabi frequency and power, data not shown) for the theory plots.

For obtaining time averages, we analyzed the curve $P_1 = P_1(t)$ to extract the minimal time t_{min} after which the oscillation amplitude has no change. And then applied averaging for the interval $[t_{\text{min}}, t_{\text{final}}]$, where t_{final} corresponds to the time of the pulse turning off. We determined that for our case $t_{\text{min}} = 1.5 \mu\text{s}$ and $t_{\text{final}} = 2.0 \mu\text{s}$.

Such interferograms are useful not only for obtaining the fitting parameters, but also they play a key role for characterizing the system. Particularly, such kind of figures:

- allow to estimate the decoherence time of the system. Consider cases (a) and (b) of Fig. 2. We see that for the case (b) the peaks are separated, while for (a) they are not distinguishable. The maximal frequency f_{pump} for which we have a smooth pic-

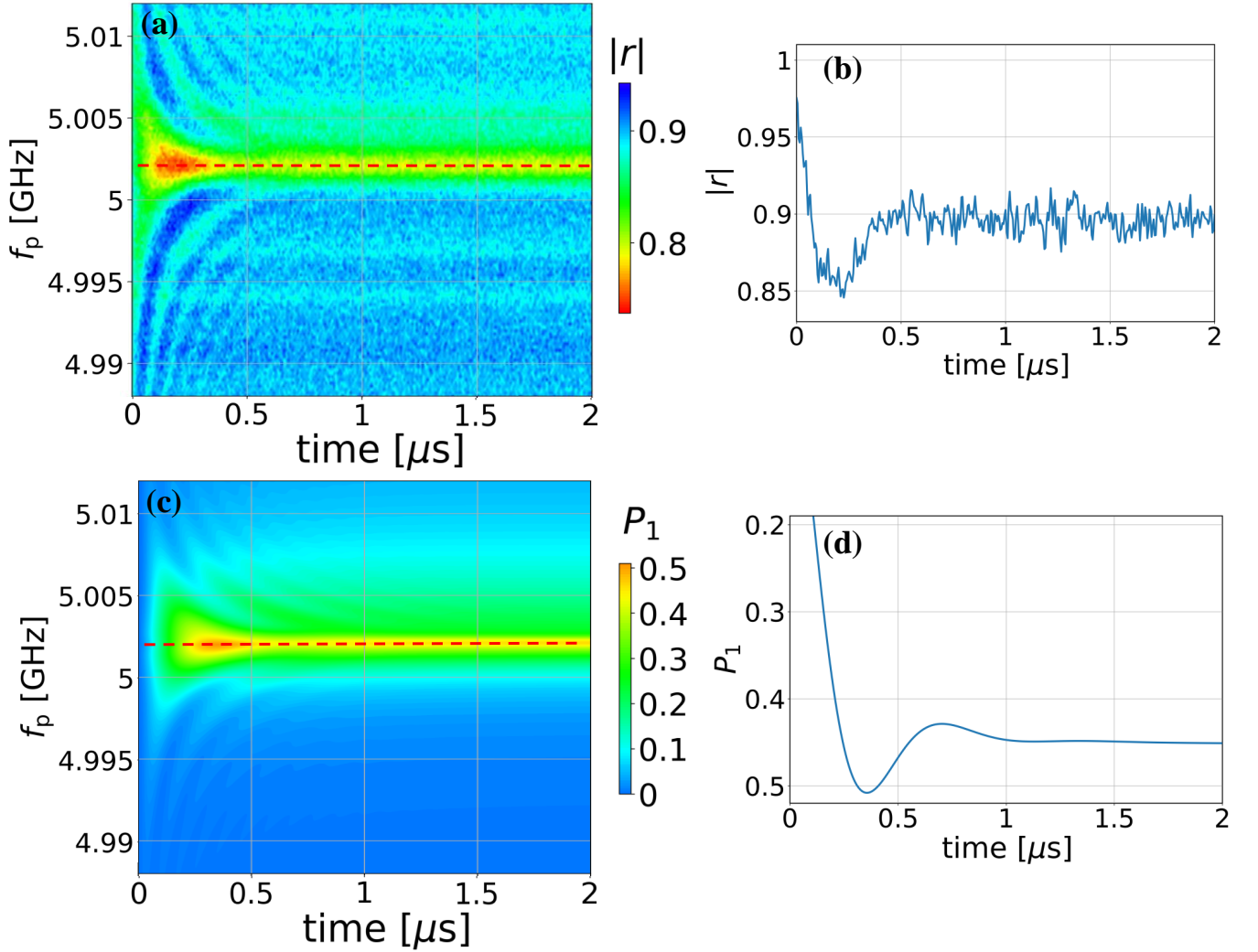


Figure 6: Coherent dynamics of the transmon qubit: dependence of the reflection coefficient $|r|$ (the upper-level occupation probability P_1) with pump off on the probe frequency f_p and time t for a weak probe $P_p = -146$ dBm [$G(f_p = 5 \text{ GHz}) = 2\pi \times 1.4 \text{ MHz}$] and $\omega_{10} = 5.002$ GHz. Plots (a, b) present experimental results; while (c, d) show plots computed theoretically. Panels (b) and (d) are line cuts of the experimental (a) and theoretical (c) plots, respectively, at $f_p = 5.002$ GHz.

ture corresponds to the system decoherence time;

- provide tools for power calibration by interrelating the zeros along the vertical axis;
- give opportunities for multi-photon spectroscopy. It can be deduced from the figures that the resonances appear when $f_p = f_{10} \pm k f_{\text{pump}}$. Or in other words, the system is resonantly excited when the dressed qubit energy gap is equal to the energy of k photons, khf_{pump} [36].

In order to see the qubit dynamics we built the dependence $P_1 = P_1(f_p, t)$ for different pump frequencies $f_{\text{pump}} = 5 \text{ MHz}$, 10 MHz , 15 MHz . The obtained pictures can be seen in Fig. 3.

Analyzing the plots, we can make several conclusions:

- as for the stationary case, the resonances are observed at $f_p = f_{10} \pm k f_{\text{pump}}$;
- the value of the reflection coefficient $|r|$ (occupation probability P_1) oscillates with period $T = 1/f_{\text{pump}}$.

All theoretical plots were built using data obtained by solving the Lindblad equation with framework QuTiP (Quantum Toolbox in Python) [41, 42]. The function `mesolve($H, \rho_0, c_{\text{ops}}, \dots$)` from this library takes the Hamiltonian H in a matrix form (in our case $H = H_1$), the initial state of the system ρ_0 (we assume that initially the system was in the ground state $|0\rangle$), set of collapse operators c_{ops} which are related to the Lindblad superoperators (11) and some other parameters. The function `mesolve($H, \rho_0, c_{\text{ops}}, \dots$)` returns elements of the density matrix ρ dependent on time.

V. CONCLUSIONS

In conclusion, we considered the dynamics and stationary regime of a capacitively-shunted transmon-type qubit in front of a mirror, affected by two signals: probe and dressing (pump) signals. The multi-photon resonance dynamics, occurring at $f_p = f_{10} \pm k f_{\text{pump}}$, consists of two regimes of time dynamics: transient and stationary. The occupation probability P_1 obtained by the Lindblad equation and the experimentally measured reflection coefficient $|r|$ agree well with each other. The reflection coefficient in the stationary state oscillates with period $T = 1/f_{\text{pump}}$. This work provides insight on the dynamics of LZSM interferometry.

Acknowledgments

I.-C.H. acknowledges financial support from the Research Grants Council of Hong Kong (Grant No. 11312322). J.C.C. acknowledges financial support from the NSTC of Taiwan under project 110-2112-M-007 - 022 -MY3 and 111-2119-M-007 -008. P.Y.W. acknowledges financial support from the NSTC of Taiwan under project 110-2112-M-194-006-MY3. M.P.L. and S.N.S. were supported by Army Research Office (ARO) (Grant No. W911NF2010261). F.N. is supported in part by: Nippon Telegraph and Telephone Corporation (NTT) Research, the Japan Science and Technology Agency (JST) [via the Quantum Leap Flagship Program (Q-LEAP)], and the Moonshot R&D Grant Number JP-MJMS2061], the Japan Society for the Promotion of Science (JSPS) [via the Grants-in-Aid for Scientific Research (KAKENHI) Grant No. JP20H00134], the Army Research Office (ARO) (Grant No. W911NF-18-1-0358), the Asian Office of Aerospace Research and Development (AOARD) (via Grant No. FA2386-20-1-4069), and the Foundational Questions Institute Fund (FQXi) via Grant No. FQXi-IAF19-06.

Appendix A: Time dynamics of an atom-mirror system irradiated by probe and dressing (pump) signals

Here we consider one more case of studying the time dynamics of the atom-mirror system irradiated by probe and dressing (pump) signals. One possible approach involves fixing the probe frequency f_p and analyzing the reflection coefficient $|r|$ as function of time t , as shown in Fig. 4. The measurements and calculations were done for various values of the pump frequency $f_{\text{pump}} = 5 \text{ MHz}$, 10 MHz , 15 MHz , with $f_p = 5 \text{ GHz}$. From the analysis of the plots one could conclude that:

- the probability and the reflection coefficient oscillate with period $T = 1/f_{\text{pump}}$;
- for the pumping frequency, $f_{\text{pump}} = 5 \text{ MHz}$, there are two kinds of peaks: high and low ones;
- the system dynamics consists of two regimes: stationary and transient ones. The stationary regime is observed after $t = 1.5 \mu\text{s}$ for all the cases considered.

Figure 5 shows the dependence of the reflection coefficient $|r|$ as a function of the probe frequency f_p and time t . The measurements and calculations were done for various values of the pump power P_{pump} (δ in the theory) and fixed pump frequency $f_{\text{pump}} = 10 \text{ MHz}$. From the plots we can deduce that increasing the pump power amplifies the resonances.

To understand better the influence of the pump signal on the system dynamics, we show the plots with no flux pump. The corresponding results with $\delta = 0$ and $\omega_{10} = 5.002 \text{ GHz}$ (in this case ω_{10} is slightly changed due to a slightly different flux bias) are shown in Fig. 6. Panel (a) shows the dependence of the reflection coefficient $|r|$ on time t and probe frequency f_p , (c) is the corresponding theoretical result; panel (b) is the line cut of (a) at $f_p = 5.002 \text{ GHz}$, and (d) is the corresponding theoretical curve.

* These authors contributed equally to this work

† e-mail:liul@ilt.kharkov.ua; These authors contributed equally to this work

‡ e-mail:iochoi@cityu.edu.hk

¹ M. A. Nielsen and I. L. Chuang, *Quantum Computation and Quantum Information: 10th Anniversary Edition* (Cambridge University Press, 2010).

² H. Haffner, C. Roos, and R. Blatt, "Quantum computing with trapped ions," *Phys. Rep.* **469**, 155–203 (2008).

³ F. Arute *et al.*, "Quantum supremacy using a programmable superconducting processor," *Nature* **574**, 505 (2019).

⁴ I. Buluta, S. Ashhab, and F. Nori, "Natural and artificial atoms for quantum computation," *Rep. Prog. Phys.* **74**, 104401 (2011).

⁵ M. Kjaergaard, M. E. Schwartz, J. Braumüller, P. Krantz,

J. I.-J. Wang, S. Gustavsson, and W. D. Oliver, "Superconducting qubits: Current state of play," *Annu. Rev. Condens. Matter Phys.* **11**, 369 (2020).

⁶ A. F. Kockum and F. Nori, "Quantum Bits with Josephson Junctions," in *Fundamentals and Frontiers of the Josephson Effect* (Springer International Publishing, 2019) pp. 703–741.

⁷ X. Gu, A. F. Kockum, A. Miranowicz, Y.-X. Liu, and F. Nori, "Microwave photonics with superconducting quantum circuits," *Phys. Rep.* **718-719**, 1–102 (2017).

⁸ J. M. Gambetta, J. M. Chow, and M. Steffen, "Building logical qubits in a superconducting quantum computing system," *npj Quantum Information* **3**, 2 (2017).

⁹ C. Wang *et al.*, "Towards practical quantum computers: transmon qubit with a lifetime approaching 0.5 milliseconds," *npj Quantum Information* **8**, 3 (2022).

- ¹⁰ W. D. Oliver and P. B. Welander, “Materials in superconducting quantum bits,” *MRS Bulletin* **38**, 816 (2013).
- ¹¹ D. L. Campbell, Y.-P. Shim, B. Kannan, R. Winik, D. K. Kim, A. Melville, B. M. Niedzielski, J. L. Yoder, C. Tahan, S. Gustavsson, and W. D. Oliver, “Universal nonadiabatic control of small-gap superconducting qubits,” *Phys. Rev. X* **10**, 041051 (2020).
- ¹² E. Lucero, R. Barends, Y. Chen, J. Kelly, M. Mariantoni, A. Megrant, P. O’Malley, D. Sank, A. Vainsencher, J. Wenner, T. White, Y. Yin, A. Cleland, and J. Martinis, “Computing prime factors with a Josephson phase qubit quantum processor,” *Nat. Phys.* **8**, 719 (2012).
- ¹³ I.-C. Hoi, A. F. Kockum, L. Tornberg, A. Pourkabirian, G. Johansson, P. Delsing, and C. M. Wilson, “Probing the quantum vacuum with an artificial atom in front of a mirror,” *Nat. Phys.* **11**, 1045–1049 (2015).
- ¹⁴ K. Lalumiere, B. C. Sanders, A. F. van Loo, A. Fedorov, A. Wallraff, and A. Blais, “Input-output theory for waveguide QED with an ensemble of inhomogeneous atoms,” *Phys. Rev. A* **88**, 043806 (2013).
- ¹⁵ A. Blais, S. M. Girvin, and W. D. Oliver, “Quantum information processing and quantum optics with circuit quantum electrodynamics,” *Nat. Phys.* **16**, 247–256 (2020).
- ¹⁶ P. Y. Wen, A. F. Kockum, H. Ian, J. C. Chen, F. Nori, and I.-C. Hoi, “Reflective amplification without population inversion from a strongly driven superconducting qubit,” *Phys. Rev. Lett.* **120**, 063603 (2018).
- ¹⁷ X. Xu, B. Sun, P. R. Berman, D. G. Steel, A. S. Bracker, D. Gammon, and L. J. Sham, “Coherent optical spectroscopy of a strongly driven quantum dot,” *Science* **317**, 929–932 (2007).
- ¹⁸ F. Y. Wu, S. Ezekiel, M. Ducloy, and B. R. Mollow, “Observation of amplification in a strongly driven two-level atomic system at optical frequencies,” *Phys. Rev. Lett.* **38**, 1077–1080 (1977).
- ¹⁹ M. Mirhosseini, E. Kim, X. Zhang, A. Sipahigil, P. B. Dieterle, A. J. Keller, A. Asenjo-Garcia, D. E. Chang, and O. Painter, “Cavity quantum electrodynamics with atom-like mirrors,” *Nature* **569**, 692 (2019).
- ²⁰ P. Y. Wen, K.-T. Lin, A. F. Kockum, B. Suri, H. Ian, J. C. Chen, S. Y. Mao, C. C. Chiu, P. Delsing, F. Nori, G.-D. Lin, and I.-C. Hoi, “Large collective Lamb shift of two distant superconducting artificial atoms,” *Phys. Rev. Lett.* **123**, 233602 (2019).
- ²¹ I.-C. Hoi, T. Palomaki, J. Lindkvist, G. Johansson, P. Delsing, and C. M. Wilson, “Generation of nonclassical microwave states using an artificial atom in 1D open space,” *Phys. Rev. Lett.* **108**, 263601 (2012).
- ²² C. M. Wilson, G. Johansson, A. Pourkabirian, M. Simoen, J. R. Johansson, T. Duty, F. Nori, and P. Delsing, “Observation of the dynamical Casimir effect in a superconducting circuit,” *Nature* **479**, 376–379 (2011).
- ²³ I.-C. Hoi, A. F. Kockum, T. Palomaki, T. M. Stace, B. Fan, L. Tornberg, S. R. Sathyamoorthy, G. Johansson, P. Delsing, and C. M. Wilson, “Giant Cross-Kerr effect for propagating microwaves induced by an artificial atom,” *Phys. Rev. Lett.* **111**, 053601 (2013).
- ²⁴ I.-C. Hoi, C. M. Wilson, G. Johansson, T. Palomaki, B. Peropadre, and P. Delsing, “Demonstration of a single-photon router in the microwave regime,” *Phys. Rev. Lett.* **107**, 073601 (2011).
- ²⁵ D. Karpov, V. Monarkha, D. Szombati, A. Friero, A. Omelyanchouk, E. Il’ichev, A. Fedorov, and S. Shevchenko, “Probabilistic motional averaging,” *Eur. Phys. J. B* **93**, 49 (2020).
- ²⁶ W. D. Oliver, Y. Yu, J. C. Lee, K. K. Berggren, L. S. Levitov, and T. P. Orlando, “Mach-Zehnder interferometry in a strongly driven superconducting qubit,” *Science* **310**, 1653–1657 (2005).
- ²⁷ M. Sillanpää, T. Lehtinen, A. Paila, Y. Makhlin, and P. Hakonen, “Continuous-time monitoring of Landau-Zener interference in a Cooper-pair box,” *Phys. Rev. Lett.* **96**, 187002 (2006).
- ²⁸ S. N. Shevchenko, S. Ashhab, and F. Nori, “Landau-Zener-Stückelberg interferometry,” *Phys. Rep.* **492**, 1–30 (2010).
- ²⁹ O. V. Ivakhnenko, S. N. Shevchenko, and F. Nori, “Nonadiabatic Landau-Zener-Stückelberg-Majorana transitions, dynamics and interference,” *Phys. Rep.* **995**, 1–89 (2023).
- ³⁰ L. Y. Gorelik, N. I. Lundin, V. S. Shumeiko, R. I. Shekhter, and M. Jonson, “Superconducting single-mode contact as a microwave-activated quantum interferometer,” *Phys. Rev. Lett.* **81**, 2538–2541 (1998).
- ³¹ T. Wu, Y. Zhou, Y. Xu, S. Liu, and J. Li, “Landau-Zener-Stückelberg interference in nonlinear regime,” *Chin. Phys. Lett.* **36**, 124204 (2019).
- ³² S. N. Shevchenko, *Mesoscopic Physics meets Quantum Engineering* (World Scientific, Singapore, 2019).
- ³³ P. O. Kofman, O. V. Ivakhnenko, S. N. Shevchenko, and F. Nori, “Majorana’s approach to nonadiabatic transitions validates the adiabatic-impulse approximation,” [arXiv:2208.00481](https://arxiv.org/abs/2208.00481) (2022).
- ³⁴ M. P. Liul and S. N. Shevchenko, “Rate-equation approach for multi-level quantum systems,” *Low Temp. Phys.* **49**, 102–108 (2023).
- ³⁵ A. M. Satanin, M. V. Denisenko, S. Ashhab, and F. Nori, “Amplitude spectroscopy of two coupled qubits,” *Phys. Rev. B* **85**, 184524 (2012).
- ³⁶ P. Y. Wen, O. V. Ivakhnenko, M. A. Nakonechnyi, B. Suri, J.-J. Lin, W.-J. Lin, J. C. Chen, S. N. Shevchenko, F. Nori, and I.-C. Hoi, “Landau-Zener-Stückelberg-Majorana interferometry of a superconducting qubit in front of a mirror,” *Phys. Rev. B* **102**, 075448 (2020).
- ³⁷ W.-J. Lin *et al.*, “Deterministic loading of microwaves onto an artificial atom using a time-reversed waveform,” *Nano Lett.* **22**, 8137–8142 (2022).
- ³⁸ S. Probst, F. B. Song, P. A. Bushev, A. V. Ustinov, and M. Weides, “Efficient and robust analysis of complex scattering data under noise in microwave resonators,” *Rev. Sci. Instrum.* **86**, 024706 (2015).
- ³⁹ M. Silveri, K. Kumar, J. Tuorila, J. Li, A. Vepsäläinen, E. Thuneberg, and G. Paraoanu, “Stueckelberg interference in a superconducting qubit under periodic latching modulation,” *New J. Phys.* **17**, 043058 (2015).
- ⁴⁰ K. Ono, S. N. Shevchenko, T. Mori, S. Moriyama, and F. Nori, “Analog of a quantum heat engine using a single-spin qubit,” *Phys. Rev. Lett.* **125**, 166802 (2020).
- ⁴¹ J. Johansson, P. Nation, and F. Nori, “QuTiP: An open-source Python framework for the dynamics of open quantum systems,” *Comput. Phys. Commun.* **183**, 1760–1772 (2012).
- ⁴² J. Johansson, P. Nation, and F. Nori, “QuTiP 2: A Python framework for the dynamics of open quantum systems,” *Comput. Phys. Commun.* **184**, 1234–1240 (2013).